An Efficient Method for Porosity Properties Extraction of Carbonate Rocks

Victor G. Cardoso*, Edna N. S. Barros†
Center of Informatics
Federal University of Pernambuco
Recife, Pernambuco - Brazil
*victor.cardoso@ufpe.br, †ensb@cin.ufpe.br

José A. Barbosa
Department of Geology
Federal University of Pernambuco
Recife, Pernambuco - Brazil
jose.antoniob@ufpe.br

Antonio D. Antonino‡, Abraão V. Nova§
Department of Nuclear Energy
Federal University of Pernambuco
Recife, Pernambuco - Brazil
{‡acda, §abraao.vilanova}@ufpe.br

***Abstract*—Porous media characterization presents substantial importance for the oil industry. The X-ray micro-computed tomography (μCT) is often used to generate digital models of reservoir rocks. This paper presents an automatic histogram-based method for the segmentation of μ CT images, which allows the fast extraction of some petrophysical properties. The processing is based on the analysis of the typical 2D images used to produce 3D volumes. The method was applied to analyze seven samples of carbonate rocks, to define the porosity values, pores size distribution, and the orientation of the pores. Calculated porosity values were compared to the porosity results obtained with a helium porosimeter. The comparison of porosity calculated by this method against the experimental values showed an average error of 3.43%. The computational time spent for each sample processing was of about 9 minutes on a regular PC. The method can be used to extract porosity parameters in a large number of samples with a substantial gain of time and computational power.**

I. Introduction

Petrophysical characterization of hydrocarbon reservoir rocks is of extreme importance for the oil industry. Thus, several analysis techniques used to extract these properties have been an intense research object in recent years. The modeling of porous through images obtained by X-ray micro-computed tomography (μCT) has evolved substantially and allows the generation of high-quality images and access to the internal rock structures. The present processing methods can provide quantitative data regarding many characteristics of rocks porous network [1]. Image segmentation techniques were also subject to significant development. They allow sophisticated analysis of the microstructures of rock samples, according to the application of a varied number of workflows [2]–[5]. In this field of study, some works focus on providing accurate information on the porous volume of rock samples using complex image processing techniques [6], while others focus on the extraction of detailed data about the morphology of the porous media [7]. Due to the large size of image files that can be produced, regarding the necessity of larger samples and the highest possible resolution, the existing approaches require substantial time (manual parameterization) and computing power. The present procedures provide an enormous quantity of information. However, it needs to improve its applicability to the industry demands, which involves the necessity of treating a large number of samples daily.

This part of the μCT images application has become a bottleneck for reservoir rocks' characterization. Thus, reduction of time μCT images analyses trough more efficient processing methods, capable of producing faster and reliable results represents a key challenge for the oil industry.

This work presents a method to extract some petrophysical properties of μCT images of rock samples, which represent analogs of carbonate reservoir rocks. The main objective was to reduce the computational processing of images by using an automatic procedure to reduce the processing time and computational power. The method was designed to allow an industrial processing routine, with less manual parameterization. The code was capable of extracting the porosity values (ϕ) of the imaged samples, the pore size distribution, and the pores' orientation. These characteristics are fundamental to estimate the rock storage capacity and enable a forward analysis of flow in the porous system [8].

This paper is organized as follows. Section II describes some of related works in petrophysical characterization. Section III contains a brief description of the rock samples used to validate the analyses carried out with the code, and Section IV shows the main results achieved so far. The main conclusions are presented in Section V.

II. Related Works

A comparative study presented by Chauhan et al. [5] showed that some machine learning-based algorithms (unsupervised, supervised, and ensemble clustering approaches) can extract porosity data from μCT 3D images from rock samples. Regarding the accuracy of porosity estimation, all of the techniques demonstrated good agreement with experimental values. Analysis of the computing time needed for the computation showed that some of these techniques spent hours to perform the porosity characterization, even with the support of a high-performance computer.

Nova et al. [9] showed relevant results on the quantification of the porosity of limestone and sandstone samples through microtomographic 3D images processing, helped by calibration made with gamma ray tomographic data of the rock samples. Although, despite the good correlation between computed porosity data and experimental tests, the processing

time required to extract this single property took at least 1 hour for computing of each 3D image volume.

Kong et al. [7] conducted a detailed study on the porous medium of a synthetic sample made by 3D printing, based on the analysis of μCT images in commercial software. The authors used the *watershed* algorithm as a segmentation technique to obtain the porous volume characteristics (shape, orientation and porosity values). The comparison between the calculated porosity values and porosity data obtained with helium porosimeter tests presented an RMSE error of 3.8%. These analyses showed that this algorithm is reliable to determine petrophysical properties of rocks based on μCT images. The authors do not cite information about the time required for data processing.

As stated by Guntoro et al. [1], one crucial issue of rock samples characterization consists of finding a data processing workflow that can provide porosity features efficiently and accurately. As there is currently no general solution for precise analysis of different rock samples (lithologies), techniques for extracting petrophysical properties are still in development. Deng et al. [10] proposed a new method for enhancing image segmentation of fractured limestone rocks. Their method showed better classification accuracy compared with other segmentation techniques in the same dataset.

III. Methodology

Carbonate rocks samples used in this research were collected from outcrops located in the coastal zone of the Paraíba Basin, NE Brazil. These samples represent analogs of biogenic calcareous rocks encompassing mudstones, packstones, and coquina-like microfacies, from the Tambaba Formation (Eocene), formed in reefal and lagoon systems. We have used seven cores with 3.7 cm of diameter, and heights varying from 3.7 to 7.6 cm, for the calculation of petrophysical properties (Figure 1).

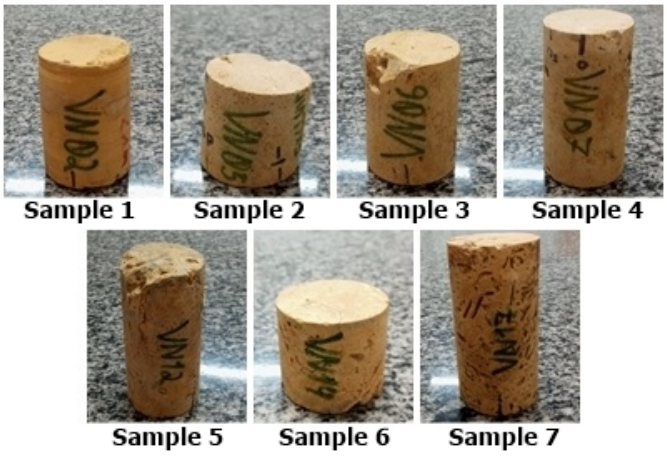

Fig. 1. Core samples used in the study ($\varnothing$ = 3.7cm).

All the samples were scanned in an X-ray micro-CT (model Nikon XT H 225 ST) with a 40 μm resolution. Scanning parameters were set at 150kV, 70μA for operating voltage and current, and the integration time was of 500 ms. An aluminum filter (0.25 mm) was used to improve image quality. After the reconstruction, the images were rescaled to Hounsfield units (16-bit images), in which air and water pixels were set to 0 and 1000, respectively.

The porosity values of the same samples were obtained through with a helium porosimeter for comparison. The new code used for image processing was developed in Python, and it operates the extraction of porosity data from the slice images created with the scanning process. The slices represent 2D images created by the reconstruction of tomographies, which are stacked vertically to build the image volume. The code loads the 2D images in memory individually during processing, and the outputs are saved in a data structure in the respective slice index, when applicable.

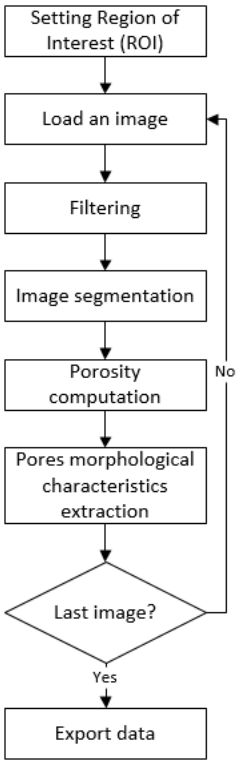

Fig. 2. Workflow diagram for the method operation.

The workflow (Figure 2) starts with the selection of the region of interest (ROI) by the system. The code selects a squared region inserted in the circular image section of each slice to reduce edge effects, which usually impacts the borders of the images (beam hardening effect) [11]. After defining the slice area, the code (Algorithm 1) carried an analysis of the first and the last slice of the selected stack of slices to project the squared area, which will fit inside all the images. In the studied cases, the square area was defined with 650 pixels of side. Due to problems with sample instability during the scanning process and irregularities in the core shape, the squared area's definition across the stacked images is systematically refined to fit all the square areas within all the

selected slices.

Algorithm 1: Selection of ROI in the images dataset.

Input: $number\_of\_images$,W
Output: $square\_coordinates$
load the first and the last slices;
apply closing operation in both images;
apply threshold segmentation in both images;
get the circumference's center (x_c, y_c) of the last slice;
while $end\_of\_algorithm$ == *False* **do**
  $number\_of\_shifts$, validation = 0;
  while *validation != 3* **do**
    while *validation == 0* **do**
      if *square's corners fits in the first slice* **then**
        validation = 1;
      else
        shift square towards the opposite direction of the failure point(s);
        $number\_of\_shifts$ += 1;
        if $number\_of\_shifts >= 20$ **then**
          break;
        end
      end
    end
    while *validation == 1* **do**
      if *square's corners fits in the last slice* **then**
        validation = 2;
      else
        shift square towards the opposite direction of the failure point(s);
        $number\_of\_shifts$ += 1;
        if $number\_of\_shifts >= 20$ **then**
          break;
        end
      end
    end
    if *square's corners, centered in* (x_c, y_c)*, fits in the first slice && validation == 2* **then**
      validation = 3;
      $end\_of\_algorithm$ = True;
    else
      validation = 0;
    end
    if $number\_of\_shifts >= 20$ **then**
      W -= 10;
      break;
    end
  end
  return $square\_coordinates$;
end

If the initial position is out of range, the system rescales the square length over the slice in at least one of the images. When the algorithm does not find a suitable region after a certain number of attempts, it reduces the square size in about 10 pixels and tries to fit it again. Figure 3 shows the representation of the clipped square area across the stacked slices (blue prismatic volume). After that, a Gaussian filter was applied to reduce noise. The method implemented for the segmentation process is based on global threshold techniques.

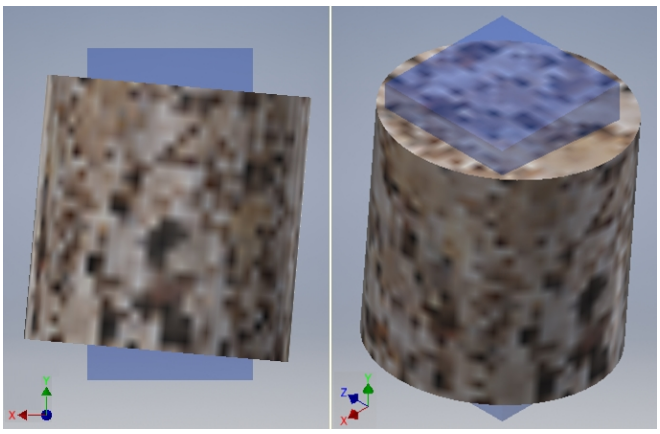

Fig. 3. Representation of the selection of Region of Interest (ROI) through the slices that composes a 3D image volume.

Although this technique can present some additional challenges for extraction of petrophysical data in the type of studied rocks, mainly caused by the microporosity, [12], [13] the validation tests with the proposed code (automated segmentation processing) showed very consistent results. Classical segmentation is based on the empirical determination of threshold values, and it depends typically on porosity measurements produced with experimental techniques for validation and verification of accuracy [13].

The new algorithm performs image segmentation based on the histogram analysis and the automatic definition of the threshold value considering the levels detected in the data. The heuristics used in this method is based on the assumption that it is a bimodal representation, and the threshold value will be at some point in the upward slope of the second peak of the histogram. These premises were previously discussed in other works, which have tested this type of analysis [14].

Algorithm 2: Computing the threshold value based on histogram data.

Input: image
Output: threshold value (thresh)
get the vector $(h(x))$ from image's histogram;
h_{max} = **max**(h);
x1 = **min**(x) $\forall$ h(x)$\geq h_{max} * l1$;
x2 = **min**(x) $\forall$ h(x)$\geq h_{max} * l2$;
thresh = $\frac{x1+x2}{2}$;
return thresh;

The algorithm operation is based on the definition of a vector $(h(x))$ for each image, where h corresponds to the number of pixels present in the image, with a given radiodensity value (x). The algorithm requires two parameters $l1$

and $l2$, to determine the threshold value. These parameters must be a real number in the interval of $0<l1<l2<1$. The lower limit ($l1$) and upper limit ($l2$) impact the interval in which the threshold value belongs. Once these parameters are determined, the threshold value is defined for each image (2D slices). The threshold value calculation is done according to the rationale presented in Algorithm 2. For defining the most suitable parameters, a series of tests are performed to compare the porosity results obtained with the automatic definition of threshold limits and the porosity values obtained through laboratory experiments.

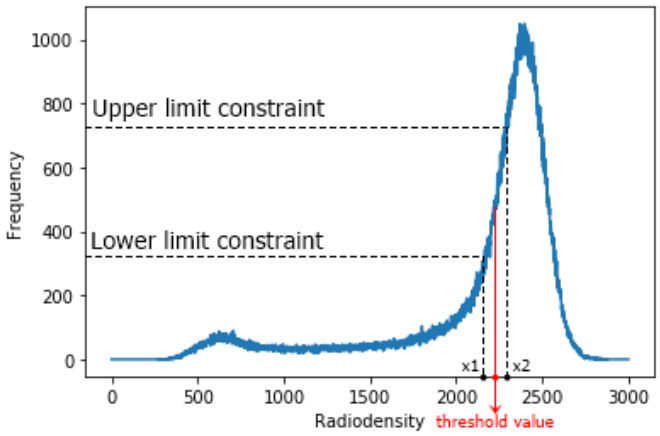

Fig. 4. Heuristics used for the threshold definition on the image Histogram. The dashed lines show how the lower and upper limits' constraints impact the determination of the threshold value (red mark).

After the automatic testing and adjustments, the analyses of porosity parameters are performed and integrated. The pores' orientation (widest axis) in each slice is calculated by considering the coordinates of the bounding boxes applied for each pore detected. The algorithm divides the oblong pores into three categories according to their specific area. To test the capacity of the algorithm of extracting porosity data with less information we have performed Sensitivity tests. That focus on the observation of the impact of reducing the number of slices from the original total dataset used to calculate porosity. We reran the analysis for each sample with 50%, 25%, 20%, 10%, and 5% of the slices from the original volume processed. These reruns were performed by loading a new set of 2D slices equally spaced in the images stack according to the percentage defined (Figure 5).

IV. Results and Discussion

A. Porosity estimation

The amount of data processed varied according to the length of each sample scanned (see Figure 1). The number of slices processed for each sample varied from 640 to 1440. Table I shows the number of slices processed for each sample and the ROI automatically defined for each set of slices. These two attributes directly reflect the proportionality of analyzed data compared to the total volume of the samples.

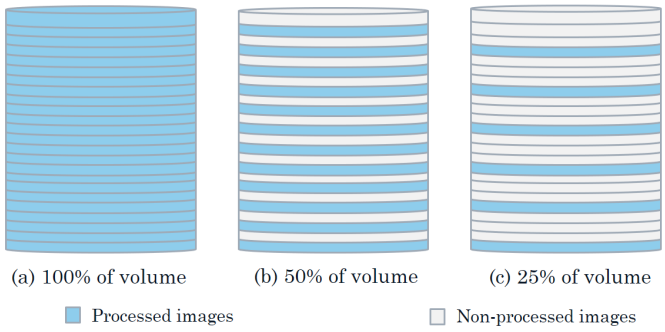

Fig. 5. Scheme showing the resampling method of slices from the original stack to perform sensitivity tests (a) 100% of the volume, (b) 50% of the volume and (c) 25% of the volume.

The segmentation step proceeded with preliminary tests to determine the percentage of the histogram's upward slope used to define the threshold limit. The consistency of the post-segmentation results was verified through the analysis of the error associated with the extracted porosity value and visual inspection. After the verification phase, the lower ($l1$) and upper limits ($l2$) were assigned to be 0.3 and 0.7. These parameters allowed the determination of the threshold value at approximately 50% of the rising edge of the second peak in the histogram. Porosity values obtained after processing are shown in Table I. The calculated porosity values were compared with the helium porosimeter tests for the rock samples. The average error was about 3.43%, and the root-mean-square error (RMSE) was about 4.47%.

TABLE I
Comparison of Porosity Values Calculated with the New Method and Obtained with Helium Porosimetry

Sample	Slices	ROI Size	Porosity (%)		Error
			Method	Porosimeter	
Sample 1	1250	630x630	13.71	16.17	-2.46
Sample 2	700	650x650	15.30	24.38	-9.08
Sample 3	1200	640x640	21.31	27.29	-5.98
Sample 4	1370	650x650	17.64	21.05	-3.41
Sample 5	1350	640x640	23.47	22.71	0.76
Sample 6	640	650x650	24.91	24.39	0.52
Sample 7	1440	640x640	26.99	25.21	1.78

The comparison of values with the porosimeter test showed differences between 0.5% to 3.4%, representing a good result except for samples 2 and 3. The higher divergence observed for the values extracted for samples 2 and 3 could be attributed to the effect of different techniques applied for the porosity data extraction. The porosimeter test accessed all the volume of the samples, and the algorithm selected a rectangular prismatic volume (ROI) within the sample scanned volume (Figure 3). Another factor that could have impacted the measurements is the microporosity, representing the porosity below the CT scanning resolution. Compared to the porosimeter tests, the best results obtained with samples 5, 6 and 7 possess a higher

TABLE II
COMPARISON OF POROSITY VALUES OBTAINED FOR THE SEVEN SAMPLES BY THE APPLICATION OF CLASSICAL METHODS OF HISTOGRAM SEGMENTATION AGAINST THE RESULTS OBTAINED WITH THE NEW METHOD.

Segmentation technique	Sample 1		Sample 2		Sample 3		Sample 4		Sample 5		Sample 6		Sample 7	
	ϕ (%)	Error	ϕ (%)	Error	ϕ (%)	Error	ϕ (%)	Error	ϕ (%)	Error	ϕ (%)	Error	ϕ (%)	Error
G. Thresh.	5.55	-10.62	22.52	-1.86	23.02	-4.27	17.06	-3.99	21.90	-0.81	21.22	-3.17	24.82	-0.39
Otsu	39.27	23.10	18.63	-5.75	8.23	-19.06	8.27	-12.78	15.83	-6.88	14.09	-10.30	8.91	-16.30
K-means	37.30	21.13	20.88	-3.50	16.95	-10.34	18.56	-2.49	18.05	-4.66	17.89	-6.50	14.06	-11.15
Prop. Method	13.71	-2.46	15.30	-9.08	21.31	-5.98	17.64	-3.41	23.47	0.76	24.91	0.52	26.99	1.78

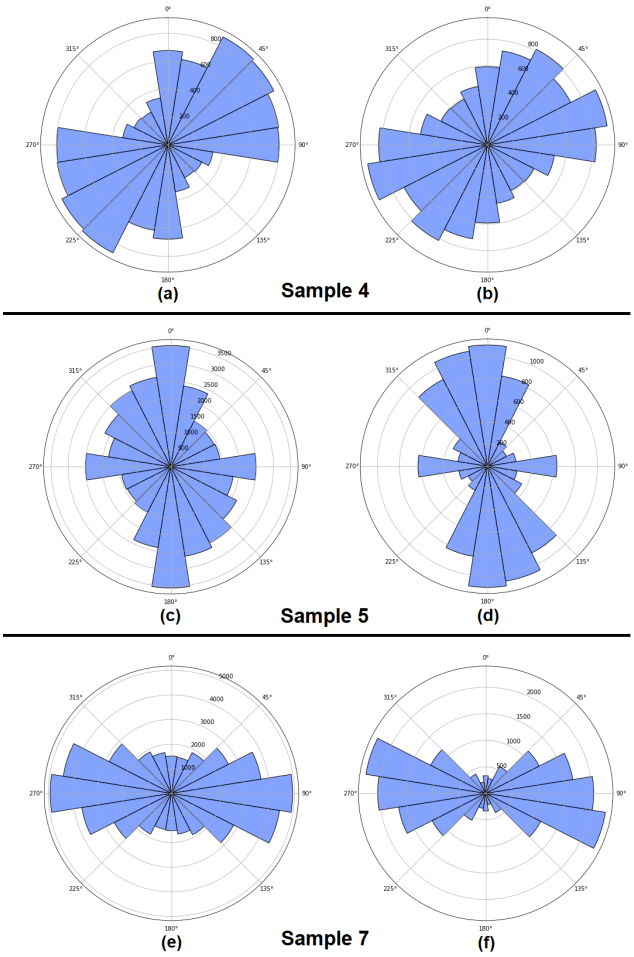

Fig. 6. Results for pores major orientation considering the distribution of large. (a), (c) and (e) represent the results obtained with the proposed approach and (b), (d) and (f) results obtained with the application of Otsu's method on ImageJ, for samples 4, 5 and 7, respectively.

proportion of the porosity of larger pores. Additionally, the code was used to determine the morphological characteristics of the pore space. The orientation of the pores in each slice was calculated, considering their specific size category, and this information was integrated between the slices. A rose diagram was automatically generated for each sample to show the orientation and distribution of pores with areas bigger than 1200 (μm^2). This area constraint can be adjusted according to the more significant contribution of larger pores on the fluid flow and rock stiffness.

As a matter of comparison, we used other segmentation techniques, commonly applied on rock characterization studies [1], [15], for the extraction of porosity values in the processed prismatic image volumes (Table II). We tested the conventional Global thresholding, Otsu's method, and K-means clustering techniques because they are commonly applied to rock characterization, request lower computing time, and do not demand intense parameterization for implementation [16]. A comparison of porosity values extracted with these segmentation methods against porosimeter tests showed poor results. These techniques are less useful for the petrophysical analysis of carbonate rocks regarding the inherent problems they present for image processing [13]. The proposed method presented better results, considering the error per sample, and the average variation, compared to experimental tests. The proposed method also showed better performance to the intrinsic aspects of the calcareous rocks treated. If necessary preprocessing algorithms Schluter et al. [17] can be applied to the images to enhance the results obtained by the new algorithm.

B. Pore orientation

Figure 6 shows the primary orientation of oblong pores, that form the major part of the porous volumes, considering their widest axis for three samples (4, 5, and 7). We used the software ImageJ [18], to calculate the area and orientation of the pores in the same image sets. The chosen segmentation technique was the Otsu's method, as it has been proven to be a well-established method for pore morphology characterization [10]. Comparison of results automatically calculated with our code against results calculated with ImageJ showed a very satisfactory correlation for both determination of large pores orientation (Figure 6). This information is essential to define aspects related to flow anisotropy and mechanical properties of the rocks [7]. According to Griffiths et al. [19], the existence of a dominant pore orientation has an essential role in determining the strength and stiffness of the rock. Consequently, these parameters are directly related to permeability.

C. Pore size distribution

The proposed code also can automatically extract the pore size distribution. This attribute provides an estimation of pores involved in the formation of porous volume according to their size, which can be separated into a few significant classes. Some studied samples presented particularities essential to verify the robustness of the method. For example, Sample 1

TABLE III

RESULTS FOR POROSITY CALCULATION OF EACH SAMPLE, WITH A REDUCED SET OF SLICES (50%, 25%, 20%, 10%, AND 5%) FROM THE ORIGINAL SET (100%). THE TEST WAS DESIGNED TO VERIFY THE ROBUSTNESS OF THE METHOD WHEN APPLIED TO ONLY A PART OF THE FULL IMAGES DATASET.

Data fraction	Sample 1		Sample 2		Sample 3		Sample 4		Sample 5		Sample 6		Sample 7	
	ϕ (%)[1]	Time[2]	ϕ (%)[1]	Time[2]	ϕ (%)[1]	Time[2]	ϕ (%)[1]	Time[2]	ϕ (%)[1]	Time[2]	ϕ (%)[1]	Time[2]	ϕ (%)[1]	Time[2]
100%	13.71	12:48	15.30	6:47	21.31	10:54	17.64	13:20	23.47	8:27	24.91	4:24	26.99	10:10
50%	13.72	5:30	15.31	3:11	21.32	5:01	17.62	6:08	23.46	2:58	24.90	2:01	27.01	4:33
25%	13.70	2:56	15.30	1:31	21.31	2:26	17.60	3:01	23.45	1:22	24.88	1:08	27.02	2:18
20%	13.73	2:09	15.26	1:12	21.25	2:01	17.62	2:35	23.44	1:08	24.87	0:49	27.00	1:54
10%	13.72	1:04	15.25	0:37	21.28	0:57	17.59	1:13	23.48	0:30	24.79	0:24	27.03	0:52
5%	13.74	0:35	15.19	0:19	21.26	0:28	17.56	0:41	23.38	0:16	24.76	0:17	27.02	0:26

[1]Porosity (%). [2]Time expressed in *min*:*sec*.

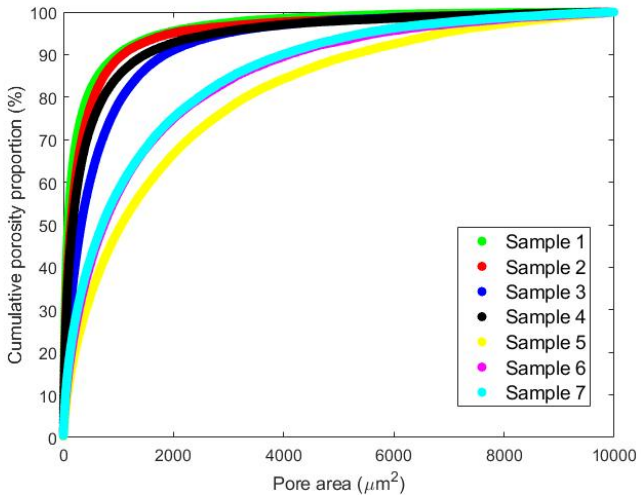

Fig. 7. Pore size distribution of the seven samples.

contains notably the smallest amount of macropores, which represents a higher contribution of micropores in the total porosity. That was likely the main reason for the unsatisfactory results of porosity measurements obtained with classical segmentation techniques. On the other hand, sample 7 possessed most important contribution of larger pores and a considerable number of elongated pores, which resulted from the dissolution of bioclasts (Figure 1).

Figure 7 shows the relationship between the cumulative porosity volume and the distribution of the pores according to their area for all samples. The samples are divided in two main groups: Group 1, formed by samples 1 to 4, presents the predominance of micro and mesopores (pore areas with less than 1200μm^2), which can correspond to more than 80% of porosity detected. Group 2, that includes samples 5 to 7, which porosity are much more influenced of macropores, with at least 40% of its porosity formed by large pores.

D. Computing time

During the study, the time spent to automatic process each sample and extract the data was recorded. The analysis of performance in terms of computing time is shown in Table IV. Processing of Sample 6 was completed in the shortest time with 4m:24s. The longest processing time was 13m:20s for sample 4. The average processing time for the extraction of petrophysical data was 9m:33s (approximately 0.49 sec/slice). Computing time is directly related to the number of slices used and the ROI square size defined for each volume of images. Vectorization techniques are considered a remarkable feature in the NumPy module, and it is used for reducing time consumption when compared to conventional for-loops in Python [20]. It can be applied with the developed code to improve computing time results. The images' processing was carried out in a computer with the following configurations: Intel i7-4500U (1,8GHz-2,4GHz), 8GB of RAM, and Nvidia Geforce 840M GPU. To perform similar tasks with the same studied data, a 3D processing platform demands much more memory.

TABLE IV

TIME COMPUTING SPENT FOR THE AUTOMATIC CALCULATION OF PETROPHYSICAL PARAMETERS OF THE SEVEN SAMPLES.

Sample	S1	S2	S3	S4	S5	S6	S7
Time*	12:48	6:47	10:54	13:20	8:27	4:24	10:10

*Time expressed in *min*:*sec*.

E. Sensitivity tests

We have performed sensitivity tests to verify the limits of the new code of extracting porosity values with a reduced number of 2D images (slices). A fraction of the original quantity of slices was used to rerun the analysis (50%, 25%, 20%, 10%, and 5%) of the original number of 2D images of the samples. Table III shows the calculated porosity values and the computational time spent for the analyses. The processing time was reduced linearly according to the reduction in the number of 2D images used. The average reduction of computing time was of 95.44% when the analysis was reduced from 100% to 5% of the original dataset for each sample (Table III).

The reduction of slices in the analysis process did not significantly resulted in loss of accuracy in the results of porosity values calculation. The maximum variation between the value porosity calculated with the original number of images and the sets with reduced numbers of slices was only 0.15% (for sample 6), with a mean standard deviation of 0.03%. Although some works have shown that porosity calculation is very dependent on changes in parameters used in

segmentation algorithms [21], the calculation of this property with the new code remained practically the same with the reduction in the number of 2D images processed.

The new method is based on a processing of 2D images, and it showed compatible results, in terms of precision, with state of the art techniques that are based in 3D segmentation processes. This approach allowed us to combine the advantage of reducing the complexity of processing, maintaining the accuracy of the results obtained from more sophisticated techniques.

V. Conclusions

This paper presented a new approach based on the histogram segmentation of 2D μCT images to calculate porosity volume, area of the pores and their orientation of limestone rock samples. The code was designed to select and calculate the properties automatically, after the loading of image data. The automatic calculated porosity values were compared with porosimeter analyses of the same samples. The comparison of calculated porosity values with the data obtained through porosimeter tests showed good results.

The study also tested a few algorithms based on histogram segmentation customarily used to perform porosity analysis μCT digital images, and the results obtained with the new code was far superior. The new method also was able to define the area and the dominant orientation of the pores, which is essential for rock porous volume characterization. We compared the information processed with the new method with the information of the area and orientation of pores extracted with a classical method (Otsu's method) performed in an open software (ImageJ), and the results are consistent and accurate. The computing time spent to perform the porosity calculation showed an average of about 9.5 minutes, which is an excellent achievement and can allow the processing of a large number of samples in a significantly shorter time when compared with the processing performed with classical segmentation methods in 3D images. The processing of limestone samples showed good improvement compared with the time spent with classical approaches based on manual segmentation of 3D images. Although the new approach has shown excellent results for some carbonate rocks, its applicability for different lithologies (other carbonate and siliciclastic facies) will demand further tests.

Acknowledgment

The authors would like to thank the research group of Imaging, Characterization and Simulation in Porous Media (ICSMP), associated to the Nuclear Energy Department, at Federal University of Pernambuco - Brazil, for all the assistance in data preparation and during the scanning operation.

References

[1] P. Guntoro, Y. Ghorbani, P.-H. Koch, and J. Rosenkranz, "X-ray microcomputed tomography (μct) for mineral characterization: A review of data analysis methods," *Minerals*, vol. 9, 03 2019.

[2] M. Porter and D. Wildenschild, "Image analysis algorithms for estimating porous media multiphase flow variables from computed microtomography data: a validation study," *Computational Geosciences*, vol. 14, pp. 15 – 30, 1 2010.

[3] H. Ramandi, P. Mostaghimi, R. Armstrong, M. Saadatfar, and W. Pinczewski, "Porosity and permeability characterization of coal: A micro-computed tomography study," *International Journal of Coal Geology*, vol. 154, 10 2015.

[4] H. Taylor, C. O'Sullivan, and W. Sim, "A new method to identify void constrictions in micro-ct images of sand," *Computers and Geotechnics*, vol. 69, 09 2015.

[5] S. Chauhan, W. Rühaak, F. Khan, F. Enzmann, P. Mielke, M. Kersten, and Sass, "Processing of rock core microtomography images: Using seven different machine learning algorithms," *Computers and Geosciences*, vol. 86, pp. "120–128", 01 2016.

[6] N. Alqahtani, F. Alzubaidi, R. T. Armstrong, P. Swietojanski, and P. Mostaghimi, "Machine learning for predicting properties of porous media from 2d x-ray images," *Journal of Petroleum Science and Engineering*, vol. 184, p. 106514, 2020.

[7] L. Kong, M. Ostadhassan, C. Li, and N. Tamimi, "Pore characterization of 3d-printed gypsum rocks: A comprehensive approach," *Journal of Materials Science*, vol. 53, p. 5063–5078, 04 2018.

[8] N. Farrell and D. Healy, "Anisotropic pore fabrics in faulted porous sandstones," *Journal of Structural Geology*, vol. 104, 09 2017.

[9] A. Nova, F. Ribeiro, P. Oliveira, D. Amancio, C. Machado, A. Carolina, M. Paixão, A. Antonino, E. Barbosa, A. Barbosa, M. Lourenço, Rodrigues, and R. Heck, "Using gammaray and x-ray computed tomography for porosity quantification of reservoir analogue rocks," *EGU General Assembly 2020*, pp. 4–8, 5 2020.

[10] H. Deng, J. Fitts, and C. Peters, "Quantifying fracture geometry with x-ray tomography: Technique of iterative local thresholding (tilt) for 3d image segmentation," *Computational Geosciences*, vol. 20, 02 2016.

[11] T. Mukunoki, J. Otani, Y. Obara, and K. Kaneko, "Artifacts of x-ray ct data in the analysis of geomaterial properties," *X-CT for Geomaterials: Soils, Concrete, Rocks*, pp. 95–101, 2004.

[12] C. Appoloni, C. Fernandes, and C. Rodrigues, "X-ray microtomography study of a sandstone reservoir rock," *Nuclear Instruments & Methods in Physics Research Section A-accelerators Spectrometers Detectors and Associated Equipment - NUCL INSTRUM METH PHYS RES A*, vol. 580, pp. 629–632, 09 2007.

[13] P. Smal, P. Gouze, and O. Rodriguez, "An automatic segmentation algorithm for retrieving sub-resolution porosity from x-ray tomography images," *Journal of Petroleum Science and Engineering*, vol. 166, 03 2018.

[14] M. Freire-Gormaly, J. Ellis, A. Bazylak, and H. Maclean, "Comparing thresholding techniques for quantifying the dual porosity of indiana limestone and pink dolomite," *Microporous and Mesoporous Materials*, vol. 207, 05 2015.

[15] H. Taud, R. Martinez-Angeles, J.-F. Parrot, and L. Hernandez-Escobedo, "Porosity estimation method by x-ray computed tomography," *Journal of Petroleum Science and Engineering*, vol. 47, pp. 209–217, 06 2005.

[16] P. Iassonov, T. Gebrenegus, and M. Tuller, "Segmentation of x-ray computed tomography images of porous materials: A crucial step for characterization and quantitative analysis of pore structures," *Water Resources Research*, vol. 45, 09 2009.

[17] S. Schlüter, A. Sheppard, K. Brown, and D. Wildenschild, "Image processing of multiphase images obtained via x-ray microtomography: A review," *Water Resources Research*, vol. 50, 04 2014.

[18] C. Schneider, W. Rasband, and K. Eliceiri, "Nih image to imagej: 25 years of image analysis," *Nature Methods*, vol. 9, 07 2012.

[19] L. Griffiths, M. J. Heap, T. Xu, C. Chen, and P. Baud, "The influence of pore geometry and orientation on the strength and stiffness of porous rock," *Journal of Structural Geology*, vol. 96, 02 2017.

[20] S. van der Walt, S. Colbert, and G. Varoquaux, "The numpy array: A structure for efficient numerical computation," *Computing in Science & Engineering*, vol. 13, pp. 22 – 30, 05 2011.

[21] L. Leu, S. Berg, F. Enzmann, R. Armstrong, and M. Kersten, "Fast x-ray micro-tomography of multiphase flow in berea sandstone: A sensitivity study on image processing," *Transport in Porous Media*, vol. 105, 09 2014.